Mid- to Low-Frequency Fourier Transform Infrared Spectra of S-State Cycle for Photosynthetic Water Oxidation in *Synechocystis* sp. PCC 6803†

Toshihiro Yamanari,§ Yukihiro Kimura,*,‡ Naoki Mizusawa,‡ Asako Ishii,‡ and Taka-aki Ono*,‡

Laboratory for Photo-Biology (1), RIKEN Photodynamics Research Center, The Institute of Physical and Chemical Research, 519-1399 Aoba, Aramaki, Aoba, Sendai 980-0845, Japan, and Faculty of Integrated Arts and Sciences, Hiroshima University, 1-7-1 Kagamiyama, Higashi-Hiroshima 739-8521, Japan

Received December 12, 2003; Revised Manuscript Received March 1, 2004

ABSTRACT: Flash-induced Fourier transform infrared (FTIR) difference spectra for the four-step S-state cycle and the effects of global ^{15}N- and ^{13}C-isotope labeling on the difference spectra were examined for the first time in the mid- to low-frequency (1200−800 cm^{-1}) as well as the mid-frequency (1700−1200 cm^{-1}) regions using photosystem (PS) II core particles from cyanobacterium *Synechocystis* sp. PCC 6803. The difference spectra clearly exhibited the characteristic vibrational features for each transition during the S-state cycling. It is likely that the bands that change their sign and intensity with the S-state advances reflect the changes of the amino acid residues and protein matrices that have functional and/or structural roles within the oxygen-evolving complex (OEC). Except for some minor differences, the trends of S-state dependence in the 1700−1200 cm^{-1} frequency spectra of the PS II cores from *Synechocystis* were comparable to that of spinach, indicating that the structural changes of the polypeptide backbones and amino acid side chains that occur during the oxygen evolution are inherently identical between cyanobacteria and higher plants. Upon ^{13}C-labeling, most of the bands, including amide I and II modes and carboxylate stretching modes, showed downward shifts; in contrast, ^{15}N-labeling induced isotopic shifts that were predominantly observed in the amide II region. In the mid- to low-frequency region, several bands in the 1200−1140 cm^{-1} region were attributable to the nitrogen- and/or carbon-containing group(s) that are closely related to the oxygen evolution process. Specifically, the putative histidine ligand exhibited a band at 1113 cm^{-1} which was affected by both ^{15}N- and ^{13}C-labeling and showed distinct S-state dependency. The light-induced bands in the 900−800 cm^{-1} region were downshifted only by ^{13}C-labeling, whereas the bands in the 1000−900 cm^{-1} region were affected by both ^{15}N- and ^{13}C-labeling. Several modes in the mid- to low-frequency spectra were induced by the change in protonation state of the buffer molecules accompanied by S-state transitions. Our studies on the light-induced spectrum showed that contributions from the redox changes of Q_A and the non-heme iron at the acceptor side and Y_D were minimal. It was, therefore, suggested that the observed bands in the 1000−800 cm^{-1} region include the modes of the amino acid side chains that are coupled to the oxidation of the Mn cluster. S-state-dependent changes were observed in some of the bands.

Photosynthetic water oxidation occurs within an oxygen-evolving complex (OEC),[1] the catalytic center of which is a tetranuclear Mn cluster that resides on the lumenal side of the D1 protein. Two water molecules are oxidized to an oxygen molecule through a light-driven reaction cycle via five intermediate states designated as S_0-S_4, where S_0 is the lowest oxidation state. When photosystem (PS) II is illuminated with a series of short flashes, the S_1-state OEC, which is thermally stable and is predominant in the dark, is oxidized to the higher S-states in a stepwise fashion by absorbing a photon at each step. After the third flash, the OEC reaches the highest oxidation state, S_4, and then subsequently decays to the lowest oxidation state, S_0, concurrent with the release of an oxygen molecule (*1*−*4*). In essence, the S-state cycling consists of a cumulative oxidation of the Mn cluster and/or its ligand, including the substrate water. In addition, it has been proposed that a Y_Z tyrosine is involved in the catalytic reaction for the water oxidation through proton-coupled electron-transfer processes that are facilitated by a H-bonding network within the protein matrices of the OEC (*3*). Structural and functional roles of inorganic cofactors, calcium and chloride ions, within the OEC have been also proposed (*1*, *5*). Although recent X-ray crystallographic studies on the structure of the OEC indicate that the four Mn ions are positioned in a trimer−monomer

† This research was supported by grants for the Frontier Research System and Special Postdoctoral Researchers Program at RIKEN and Grant-in-Aid for Young Scientists (B) (14780518) (to Y.K.) from MEXT of Japan.

* To whom correspondence should be addressed.Tel.: +81 (22) 228 2047. Fax: +81 (22) 228 2045. E-mail: ykimura@postman.riken.go.jp, takaaki@postman.riken.go.jp.

‡ RIKEN.

§ Hiroshima University.

[1] Abbreviations: FTIR, Fourier transform infrared; EPR, electron paramagnetic resonance; OEC, oxygen-evolving complex; PS, photosystem; Chl, chlorophyll; Q_A, primary quinone acceptor of photosystem II; Y_D, tyrosine 160 of the D2 protein; Y_Z, redox-active tyrosine 161 of the D1 protein; Mes, 2-morpholinoethanesulfonic acid; DCMU, 3-(3,4-dichlorophenyl)-1,1-dimethylurea; EDTA, ethylenediamine-*N*,*N*,*N*′,*N*′-tetraacetic acid.

10.1021/bi0362323 CCC: $27.50
Published on Web 05/19/2004

arrangement (*6*−*8*), the individual Mn ions, as well as amino acid ligands for the Mn cluster, have yet to be defined with high resolution. To clarify the reaction mechanism of the photosynthetic oxygen evolution in the OEC, detailed structural and functional information on the Mn cluster during the S-state cycling is indispensable. Accordingly, the S-state cycling has been intensively studied in terms of proton release (*3*), substrate water exchange (*9*), magnetic properties of the Mn cluster using EPR (*10*, *11*), structure and oxidation states of the Mn cluster using X-ray absorption (*12*, *13*), and oxidation of the donor side components using UV−visible absorption (*14*).

Essential information to help elucidate the molecular mechanism of the water oxidation can be obtained by detecting, during the reaction process of the water oxidation, changes within the chemical structures of the OEC, including the protein matrices, ligands for the Mn cluster, substrate water, inorganic cofactors, Y_Z, and hydrogen-bonding networks among these components. For this purpose, light-induced FTIR difference spectroscopy has been extensively applied toward the study of the photosynthetic oxygen evolution (*15*−*43*). It has been shown that the mid-frequency (1800−1200 cm^{-1}) S_2/S_1 FTIR difference spectra can exhibit the light-induced changes of the vibrational modes of several amino acid residues that are structurally coupled to the Mn cluster as well as amide I and amide II. These vibrational modes were assigned to the carboxylate (*16*) and histidine modes (*26*) from the putative ligands for the Mn cluster and to the tyrosine modes, reportedly of the Y_Z tyrosine (*20*, *23*). This method was also successfully applied to the study of the functional calcium (*16*, *33*, *37*) and chloride cofactors (*38*, *43*) within the OEC. Mid-frequency FTIR difference spectra for each transition during the S-state cycling have been reported for the PS II membranes of spinach (*31*) and for the PS II core particles of cyanobacterium *Thermosynechococcus elongatus* (*30*, *36*, *39*, *40*). Although similarities in the major features of each S-state spectrum were observed between the PS II samples, some distinctions were also apparent; however, the basis of the differences remains unclear. High-frequency (3800−2150 cm^{-1}) FTIR difference spectroscopy was carried out to study the S-state-dependent changes in the OH vibrational modes of water molecules that associate with the OEC (*27*, *39*).

In general, to obtain direct information on the coordination sphere of the Mn cluster, FTIR spectra were acquired in the region lower than 1000 cm^{-1}, which includes vibrational modes arising from interactions between the Mn ion and substrate water molecules as well as the Mn ion and its ligand(s) (*25*, *28*, *32*, *35*, *42*). The low-frequency (650−350 cm^{-1}) S_2/S_1 FTIR difference spectrum showed several characteristic vibrational modes; based on their downshift upon the ^{18}O-water substitution, the bands at 606 and 625 cm^{-1} have been tentatively assigned to a Mn−O−Mn cluster mode in the S_2- and S_1-states, respectively (*28*). This mode was also affected by the substitution of Sr^{2+} ions for the functional Ca^{2+} ions (*28*) and by the site-directed mutation of Asp170 in the D1 protein to His (*32*). Furthermore, low-frequency S_2/S_1 difference spectra of the universally ^{15}N- and ^{13}C-labeled *Synechocystis* allowed the assignment of the prominent band at 577(−) cm^{-1} to the Mn-ligand(s) modes and/or the cluster core modes that are not exchangeable with water molecules (*42*).

Apart from the frequency regions described above, it is possible that the mid- to low-frequency region (1200−800 cm^{-1}) can include interactions between the Mn ions and water molecules, as well as the vibrational modes from the amino acid side chains interacting with the Mn cluster (*25*, *44*, *45*). A light-induced FTIR spectrum in this frequency region was briefly reported for the PS II core particles from spinach (*25*). Other than the presence of the negative peak at approximately 850 cm^{-1}, the spectrum was relatively featureless over the range 1000−800 cm^{-1}. Although this frequency region may provide valuable information toward the understanding of the mechanism of the photosynthetic oxygen evolution, FTIR difference spectra for the S-state cycling have yet to be reported in the frequency region lower than 1200 cm^{-1}.

In the present study, we report the mid- to low-frequency (1200−800 cm^{-1}) as well as the mid-frequency (1700−1200 cm^{-1}) FTIR difference spectra corresponding to each transition during the S-state cycling in PS II core particles from *Synechocystis* sp. PCC 6803. Furthermore, the effects of universal ^{15}N- and ^{13}C-isotope labeling on the characteristic vibrational modes in the difference spectra were systematically examined. On the basis of the results, possible assignments of the bands in the mid-frequency and mid- to low-frequency regions are discussed.

MATERIALS AND METHODS

Sample Preparations. Synechocystis sp. PCC 6803 strain bearing His-tagged CP47 protein and the PS II core particles were prepared as described previously (*42*). Briefly, the transformed *Synechocystis* cells were photoheterotrophically grown in BG-11 medium supplemented with 5 mM glucose. For global ^{15}N-labeling, the culture included 10 mM $Na^{15}NO_3$ (99.5% ^{15}N-enrichment, Shoko Co., Ltd.) as the sole nitrogen source during the cell growth, while bubbled with 2% CO_2-enriched air. For global ^{13}C-labeling, the culture included 4 mM glucose-U-^{13}C (98.3% ^{13}C-enrichment, Cambridge Isotope Laboratories Inc.) as the sole carbon source, while gently bubbled with pure air that was free of CO and CO_2 (<1 ppm CO and CO_2). The harvested cells were disrupted using a Bead-Beater (Bio-Spec Products) and then solubilized with 0.8% (w/v) *n*-dodecyl-β-D-maltoside. After centrifugation, the resulting supernatant was loaded on a Ni-NTA column (Qiagen) for purification. The resulting PS II core particles were concentrated by ultrafiltration to approximately 2 mg of Chl/mL and stored in liquid N_2. The O_2-evolution activity of the obtained PS II core particles was approximately 2500 μmol of O_2 (mg of Chl)$^{-1}$ h^{-1} at 25 °C with 4 mM potassium ferricyanide as the electron acceptor. For FTIR measurements, the sample medium was replaced with medium A (40 mM sucrose, 5 mM NaCl, 5 mM $CaCl_2$, and 10 mM Mes/NaOH, pH 6.0) using repeated ultrafiltration in the presence of 0.06% (w/v) *n*-dodecyl-β-D-maltoside, and the core particles were concentrated to approximately 3 mg of Chl/mL. In some cases, the PS II core particles were precipitated using 10% (w/v) polyethylene glycol 6000, and suspended in medium A after extensive washes with the same medium. For the Mn depletion, the PS II core particles from *Synechocystis* were treated with 5 mM NH_2OH at 0 °C for 1 min under darkness and then washed twice with medium B (0.4 M sucrose, 20 mM NaCl, 20 mM Mes/NaOH, pH 6.5) in the presence of 0.5 mM EDTA. The resulting Mn-

depleted PS II core particles were further washed twice with medium B and stored in liquid N_2 until use. PS II core particles of spinach were prepared from the BBY-type PS II membranes (*46*, *47*) by solubilization with *n*-heptyl-*β*-D-thioglucoside as described previously (*43*). The resulting PS II core particles were resuspended in medium C (0.4 M sucrose, 20 mM NaCl, 20 mM $CaCl_2$, 20 mM Mes/NaOH, pH 6.0) after two washes with the same medium and stored in liquid N_2 until use. The O_2-evolution activity of the spinach PS II core particles was approximately 2800 μmol of O_2 (mg of Chl)$^{-1}$ h^{-1} with 1 mM potassium ferricyanide and 0.25 mM 2,6-dichloro-*p*-benzoquinone as the electron acceptors.

Sample Preparations for FTIR Measurements. For the difference spectra between two successive S-states during the S-state cycling, sodium ferricyanide solution (1 μL, 100 mM stock) was added as an electron acceptor to the PS II core suspension (10 μL, 3−4 mg of Chl/mL). For the $S_2Q_A^-/S_1Q_A$ and Q_A^-/Q_A difference spectra, the sample suspension supplemented with 0.1 mM DCMU for $S_2Q_A^-/S_1Q_A$ spectrum or with 0.1 mM DCMU and 10 mM NH_2OH for Q_A^-/Q_A spectrum was precipitated by an ultracentrifuge (HITACHI, CS120) at 100000*g*, and the resulting pellet was resuspended with medium A to approximately 3 mg of Chl/mL. For the $Y_D^{\bullet}/Y_D$ difference spectrum, the Mn-depleted PS II core particles were suspended in medium A and subsequently incubated in the dark for 1 h in the presence of 1 M HCOONa (*20*, *21*, *29*). Next, the sample was washed twice and resuspended in medium A containing 100 mM HCOONa (3 mg of Chl/mL). The sample suspension (8 μL) was then mixed with sodium ferricyanide (2 μL, 100 mM stock). All sample suspensions were orbiculately deposited on a BaF_2 disk with a 20 mm diameter and partially dried under a stream of N_2 gas (4 °C). For measuring the Fe^{2+}/Fe^{3+} difference spectrum of the acceptor-side non-heme iron, sodium ferricyanide (10 μL, 100 mM stock) was dried on a BaF_2 disk before deposition of the Mn-depleted PS II core suspension (10 μL). After an aliquot (1 μL) of 20% (v/v) glycerol/water solution was placed adjacent to the sample for controlling the water content of PS II (*36*), the sample on the disk was covered by another BaF_2 disk with a greased Teflon spacer and then incubated in the dark for 1 h. The absorbance of the PS II sample was 0.7−1.0 at 1657 cm^{-1} for the measurements in the 1700−1080 cm^{-1} region and 0.3−0.5 at 925 cm^{-1} in the 1000−800 cm^{-1} region after the dark adaptation for 1 h. The sample temperature was maintained at 0 °C (±0.03 °C) using a homemade cryostat and a temperature controller (Chino, KP1000) (*42*).

FTIR Measurements. FTIR spectra were recorded on a Bruker IFS-66v/s spectrophotometer equipped with an MCT detector (EG&G Optoelectronics D316/6). A custom-made CdTe band-pass filter (2000−350 cm^{-1}) was placed in front of the sample to block any leaks of the He−Ne laser beam from the interferometer compartment. To obtain a high-quality spectrum, the spectra for the 1700−1080 and 1000−800 cm^{-1} regions were measured using custom-made Ge long-pass ≥6- and ≥9.5-μm filters, respectively. The filter was placed at the exit hole of the cryostat to protect the detector element from the scattering of laser flashes for the sample excitation, but the other experimental conditions were identical in the spectral measurements for the 1700−1080 and 1000−800 cm^{-1} regions. For the measurement of a flash-induced difference spectrum of each transition during the S-state cycling, a dark-adapted sample was pre-flashed to reduce the oxidized non-heme iron at the acceptor side and to enrich the S_1 population. After the subsequent incubation in the dark for 5 min, the sample was subjected to eight successive flashes with 12-s intervals; single-beam spectra (5 scans during 2 s) were measured before the first flash and after each flash, followed by the dark adaptation of the sample for 30 min. This sequence was repeated 4−10 times before the sample was discarded. To obtain difference spectra for respective S-state transitions, the single-beam spectrum before each flash was subtracted from that after the flash. Spectra obtained for 6−14 samples were averaged. Single-flash-induced difference spectra were obtained by subtracting the single-beam spectrum (15 scans during 7 s for the $S_2Q_A^-/S_1Q_A$ or Q_A^-/Q_A difference, 70 scans during 30 s for the $Y_D^{\bullet}/Y_D$ difference, and 25 scans during 11 s for the Fe^{2+}/Fe^{3+} difference) acquired before the flash from that after the flash. Spectra obtained for 6−12 samples were averaged. Excitation flashes were provided from a frequency-doubled Nd^{3+}:YAG laser (Spectra Physics INDI-50, 532 nm, pulse width 6−7 ns). The flash energy was approximately 10 mJ/cm^2 at the sample surface. Saturation of the light intensity of the flashes was confirmed by monitoring the amplitude of the obtained spectra and the intensities of the ferrocyanide/ferricyanide bands. All spectra were collected at 4 cm^{-1} resolution.

RESULTS

The flash-induced FTIR difference spectra in the mid-frequency region (1700−1200 cm^{-1}) during the S-state cycling of the PS II core particles from *Synechocystis* sp. PCC 6803 (black lines) and spinach (gray lines) are shown in Figure 1. The difference spectra induced by the (a) first, (b) second, (c) third, and (d) fourth flashes showed the characteristic flash-number-dependent changes of the vibrational features in the regions of asymmetric (1600−1500 cm^{-1}) and symmetric (1450−1300 cm^{-1}) carboxylate stretching modes as well as the amide I (1700−1600 cm^{-1}) and amide II (1600−1500 cm^{-1}) modes of the polypeptide backbone. These spectra were largely compatible with those previously reported for *T. elongatus* (*30*, *36*, *39*, *40*), indicating the cycling of the S-states. The characteristic vibrational features of the first- to fourth-flash spectra were also evident in the fifth- to eighth-flash spectra, although the estimated miss−hit (approximately 18%) from the oscillation pattern up to the eighth flash of several bands in the symmetric carboxylate stretching region was somewhat larger than that for *Thermosynechococcus* (*30*, *36*, *48*). The S-state dependences were observed in the *Synechocystis* spectra at 1680(−), 1670(+), 1662(−), 1651(+), 1641(−), 1622(+), 1610(−), 1587(+), 1562(−), 1543(−), 1531(+), 1522(−), 1508(+), 1438(+), 1417(−), 1400(−), 1383(−), 1363(+), 1340(+), 1325(+), 1294(−), 1271(−), and 1259(+)/1248(−) cm^{-1}, in which the bands changed their signs and intensities as the S-state advanced. Despite subtle changes in their positions and intensities, these bands exhibited S-state-dependent trends similar to those for the spinach spectra. In this context, because amide I bands tend to change rather easily depending on the sample conditions that do not strongly influence the O_2-evolving capability, it is noteworthy that some differences between the two spectra in the amide

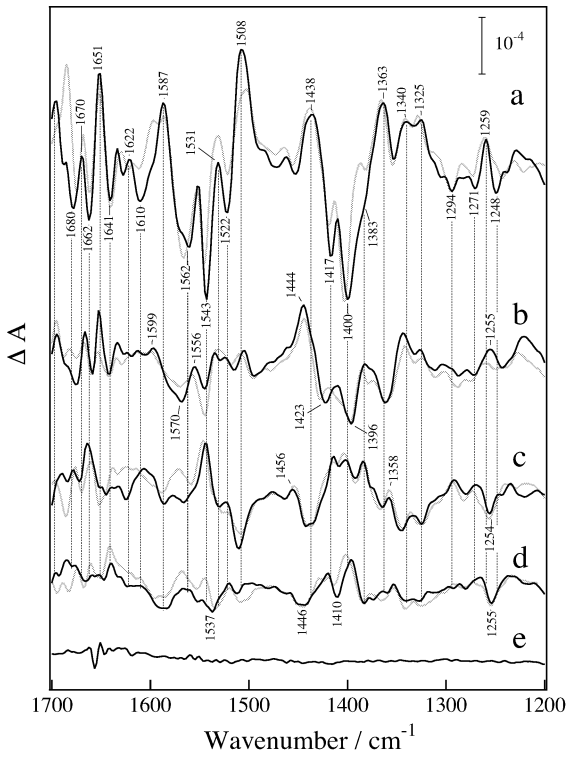

FIGURE 1: Flash-induced FTIR difference spectra in the frequency region of 1700−1200 cm^{-1} of PS II core particles from *Synechocystis* sp. PCC 6803 (black lines) and spinach (gray lines) during the S-state cycling of the OEC. (a) S_2/S_1, (b) S_3/S_2, (c) S_0/S_3, and (d) S_1/S_0 difference spectra induced upon the first-, second-, third-, and fourth-flash illumination, respectively. Samples were illuminated with a series of successive flashes provided from a frequency-doubled Nd^{3+}:YAG laser (532 nm, 6−7 ns, 10 mJ/cm^2/pulse) at 0 °C. Sample suspension included ferricyanide as an exogenous electron acceptor. Spectrum e is presented to show the noise levels. See text for other details.

I region may not reflect the fundamental differences in the OEC between the two species.

The effects of universal ^{15}N- (panel A) and ^{13}C-labeling (panel B) on the difference spectra for the S-state cycling of *Synechocystis* in the 1700−1300 cm^{-1} region are shown in Figure 2. The ^{15}N-labeled (blue lines) S_2/S_1 spectrum showed prominent isotope shifts in the amide II region (1600−1500 cm^{-1}), which includes the CN stretching and NH bending modes of the polypeptide backbone. The bands at 1574(−), 1552(+), 1543(−), and 1508(+) cm^{-1} in the unlabeled (red lines) S_2/S_1 spectrum were downshifted to 1562(−), 1537(+), 1527(−), and 1493(+) by 12−16 cm^{-1}, comparable to the downward shifts (∼16 cm^{-1}) for the amide II bands. Isotope shifts of the amide II bands were clearly observed not only in the S_2/S_1 spectrum (a) but also in the S_3/S_2 (b) and S_0/S_3 (c) spectra, accompanied with changes in the signs and intensities, indicating that the polypeptide backbone changes characteristically during the S-state transitions. In contrast, the effects of ^{15}N-labeling were not as apparent in the S_1/S_0 spectrum (d), indicating that the protein moieties represented by the amide II modes undergo minor structural changes upon the S_0-to-S_1 transition. Isotope shifts due to ^{15}N-labeling were scarcely observed through the S-state cycling in the symmetric (1450−1300 cm^{-1}) and asymmetric (1600−1500 cm^{-1}) stretching modes of the carboxylate groups; however, large isotopic bands due to the amide II modes caused ambiguity in the latter region. In contrast to the ^{15}N-labeling, most of the bands in respective S-state difference spectra were markedly affected upon ^{13}C-labeling (green lines). Since the ^{15}N-insensitive S_2/S_1 bands at 1438(+), 1417(−), 1400(−), 1383(−), and 1363(+) cm^{-1} were downshifted by 32−40 cm^{-1} upon ^{13}C-labeling, and furthermore, since similar trends were found in all the difference spectra, it is reasonable to assign these bands to the S-state-dependent symmetric stretching modes of the carboxylate groups. Similarly, upon ^{13}C-labeling, the ^{15}N-insensitive bands at 1583(−), 1568 (+), 1537(−), and 1520(+) cm^{-1} in the S_1/S_0 spectrum showed downward shifts of 34−39 cm^{-1} to 1549(−), 1529(+), 1500(−), and 1483(+) cm^{-1}, respectively, hence allowing the assignment of these bands to the asymmetric stretching modes of the carboxylate groups. Therefore, it is likely that the S_0-to-S_1 transition involves changes of the carboxylate ligands but with little structural rearrangement of the polypeptide backbone. Overall, despite some differences, the effects of the universal ^{15}N- and ^{13}C-labeling on the mid-frequency FTIR difference spectra during the S-state cycling were comparable to those reported in *Thermosynechococcus* (*40*).

The difference spectra for the S-state cycling of *Synechocystis* in the 1300−1080 cm^{-1} region and the effects of universal ^{15}N- (panel A) and ^{13}C-labeling (panel B) on the spectra are shown in Figure 3. In the unlabeled spectra (red lines), the bands at 1294(−), 1271(−), 1259(+)/1248(−), 1228(+), 1196(−), 1184(+), 1163(+), 1146(−), and 1105(+) cm^{-1} changed their signs and intensities in a flash-number-dependent manner, indicating that these bands are related to the S-state-dependent changes of the OEC. Although the overall spectral features of the ^{15}N-labeled spectra (blue lines) were relatively similar, distinct isotope shifts were also observed. Upon ^{15}N-labeling, several bands in the 1300−1200 cm^{-1} region of the S_2/S_1 spectrum exhibited slight changes in their intensities, and the bands at 1196(−), 1184(+), 1163(+), 1113(−), and 1105(+) cm^{-1} clearly showed downward shifts by 4−6 cm^{-1}. On the other hand, a majority of the S_2/S_1 bands were markedly affected by ^{13}C-labeling (green lines), suggesting that the above bands correspond to groups that contain both nitrogen and carbon atoms. Upon ^{13}C-labeling, the ^{15}N-insensitive bands at 1294(−) and 1146(−) cm^{-1} downshifted to 1269(−) and 1132(−) cm^{-1}, indicating that these bands correspond to nitrogen-free moieties.

Negative bands at 1113 cm^{-1} and near 1173 cm^{-1} were observed in the unlabeled spectra after the second, third, and fourth flashes with the same sign and intensity. A large portion of these bands were affected by neither ^{15}N- nor ^{13}C-labeling, as clearly depicted in the spectra after the fourth flash, although it is rather ambiguous in the 1173 cm^{-1} region after the second and third flashes due to the overlap of other isotopic bands. The absence of both the isotope effects and the flash-number dependency indicates that the bands at 1113 cm^{-1} and near 1173 cm^{-1} found in the second-, third-, and fourth-flash spectra are caused by some components other than those of PS II. It is of note that the 1111(−) and 1170(−) cm^{-1} bands appeared in the difference spectrum obtained by subtracting the absorption spectrum of buffer A at pH 6.0 from that at pH 5.5 (data not shown). Therefore, the isotope-insensitive bands at 1113 cm^{-1} and near 1173 cm^{-1} may be ascribed to the protonation of buffer molecules, such as Mes. Apart from the isotope-insensitive mode, the

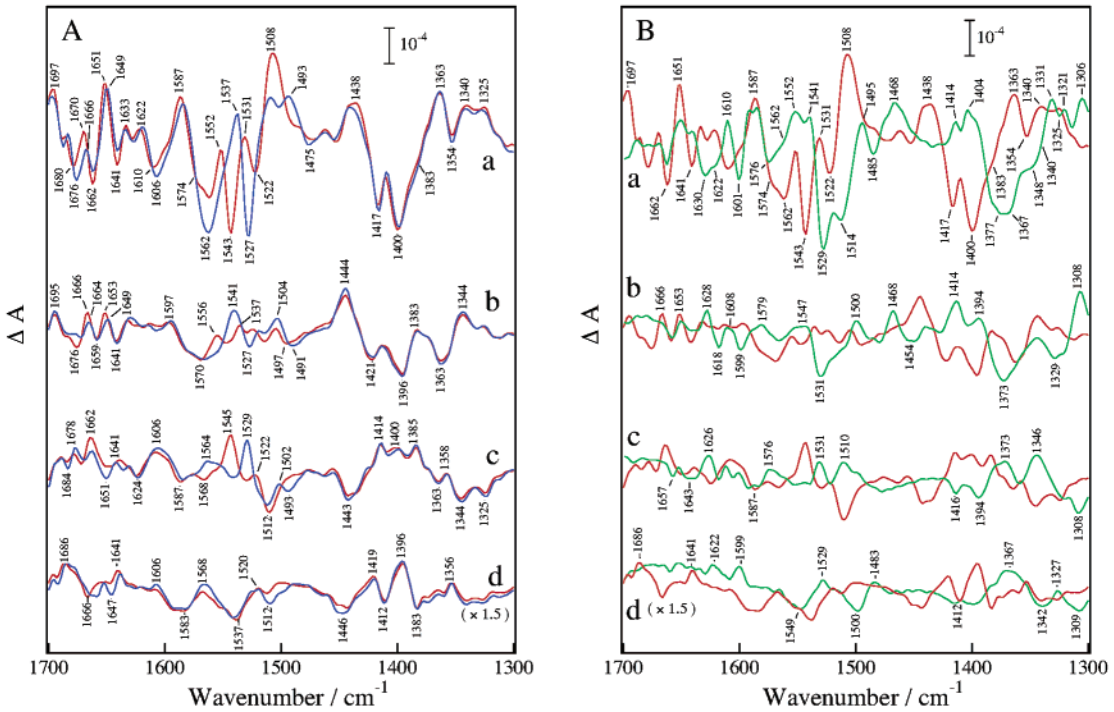

FIGURE 2: Effects of ^{15}N- (panel A) and ^{13}C-labeling (panel B) on the flash-induced FTIR difference spectra in the frequency region of 1700−1300 cm^{-1} of PS II core particles from *Synechocystis* sp. PCC 6803. (a) S_2/S_1, (b) S_3/S_2, (c) S_0/S_3, and (d) S_1/S_0 difference spectra induced upon the first-, second-, third-, and fourth-flash illumination of unlabeled (red lines), ^{15}N-labeled (blue lines), and ^{13}C-labeled (green lines) PS II core particles, respectively. Spectra d are presented after magnification in intensity by a factor of 1.5 to clarify the effects of isotopes.

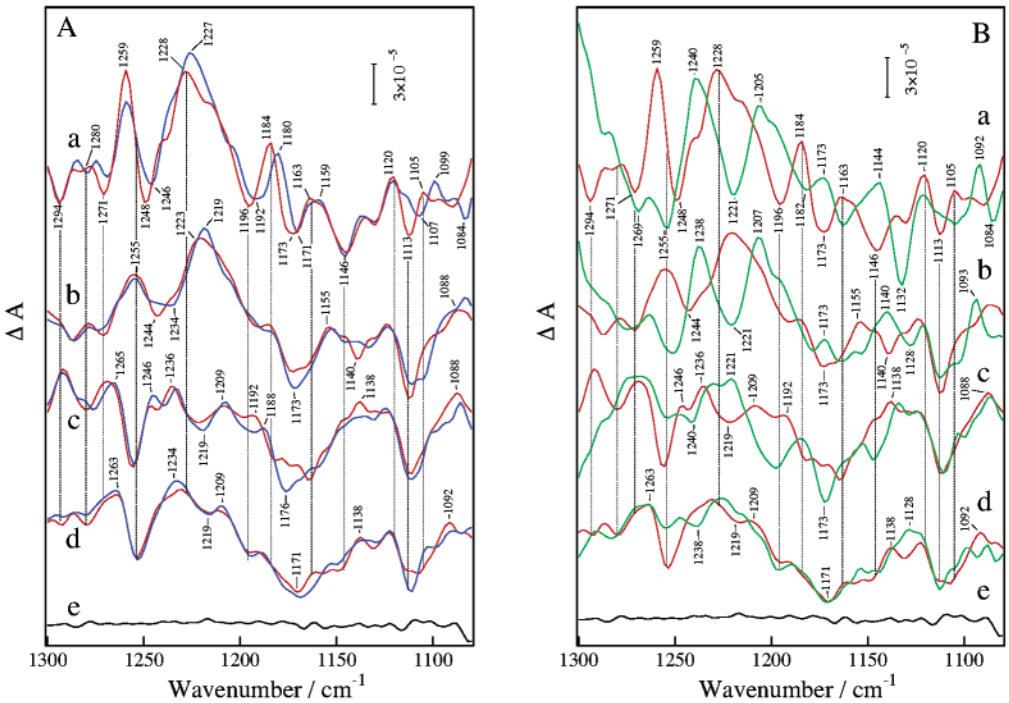

FIGURE 3: Effects of ^{15}N- (panel A) and ^{13}C-labeling (panel B) on the flash-induced FTIR difference spectra in the frequency region of 1300−1080 cm^{-1} of PS II core particles from *Synechocystis* sp. PCC 6803. (a) S_2/S_1, (b) S_3/S_2, (c) S_0/S_3, and (d) S_1/S_0 difference spectra induced upon the first-, second-, third-, and fourth-flash illumination of unlabeled (red lines), ^{15}N-labeled (blue lines), and ^{13}C-labeled (green lines) PS II core particles, respectively. Spectra e are presented to show the noise levels.

S_2/S_1 band at 1113(−) cm^{-1} was apparently downshifted to 1107(−) and 1105(−) cm^{-1} upon ^{15}N- and ^{13}C-labeling, respectively. This observation is consistent with the reported assignment of this band to the ring CN stretching mode of histidine residues that are coupled to the Mn cluster (*26*). The isotopic bands seemed to change their signs and intensities during the S-state cycling; however, the presence of the isotope-insensitive anomalous bands at 1113(−) cm^{-1} obscured the S-state-dependent changes of the isotopic bands. It is of note in this context that the present S_2/S_1 spectrum of the unlabeled *Synechocystis* does not involve the modes from the non-heme iron (*17*, *18*) and/or Q_A (*24*) that reside

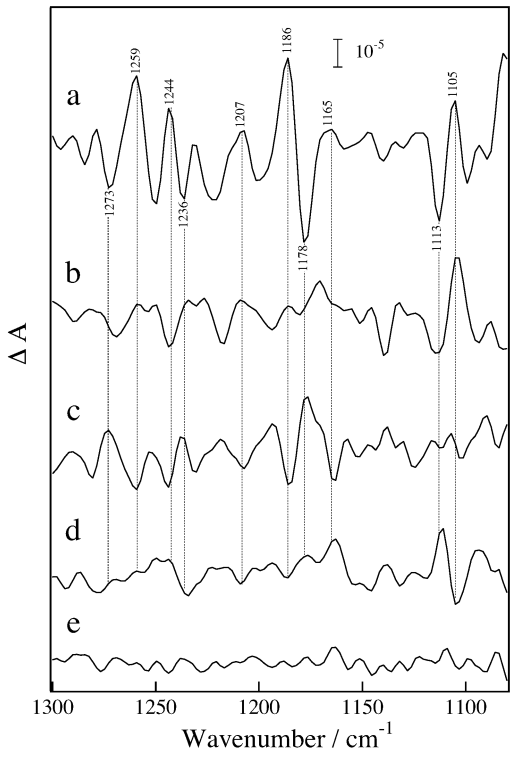

FIGURE 4: $^{14}N/^{15}N$ double-difference spectra of PS II core particles from *Synechocystis* sp. PCC 6803 for the S-state cycling. Double-difference spectra for (a) S_2/S_1, (b) S_3/S_2, (c) S_0/S_3, and (d) S_1/S_0 difference. The double-difference spectra were obtained by subtracting ^{15}N-labeled S-state difference spectra from unlabeled S-state difference spectra. Spectrum e is presented to show the noise levels for the double subtraction.

at the acceptor side of the PS II (see Figure 7A, below). These bands, therefore, do not contribute to the light-induced spectral changes of the OEC under the present experimental conditions.

The S-state dependences of the band for the putative histidine ligand as well as other bands were more clearly revealed in the $^{14}N/^{15}N$ double-difference spectra (Figure 4), which were obtained by subtracting the ^{15}N-labeled S-state difference spectra from the unlabeled S-state difference spectra. Although the resulting $^{14}N/^{15}N$ double-difference spectra allowed us to detect the S-state-dependent changes of the modes relating to nitrogen, it is difficult to explicitly determine the changes that occur in the respective bands in the S-state difference spectra. The $^{14}N/^{15}N$ double-difference spectrum for the S_2/S_1 difference (spectrum a) shows a distinct differential band at 1113(−)/1105(+) cm^{-1} that corresponds to the histidine modes at 1113(−) and 1107(−) cm^{-1} in the unlabeled and ^{15}N-labeled S_2/S_1 spectra (Figure 3A, spectra a). The band similarly appeared in the double-difference spectrum for the S_3/S_2 difference (spectrum b), indicating that the putative histidine mode changed similarly upon both S_1-to-S_2 and S_2-to-S_3 transitions; however, some differences were evident, as depicted by the smaller intensity of the 1113(−) cm^{-1} band in the S_3/S_2 double-difference spectrum than that of S_2/S_1. In contrast, the 1113(−)/1105(+) cm^{-1} bands were nearly absent in the double-difference spectrum for the S_0/S_3 difference (spectrum c), suggesting only small structural changes of the putative histidine ligand upon the S_3-to-S_0 transition or that other bands overlap with the histidine band to obscure the change. The double-difference spectrum for the S_1/S_0 difference exhibited the 1111(+)/1105(−) cm^{-1} bands, which showed the opposite sign as compared to the corresponding bands for the S_2/S_1 and S_3/S_2. It is, therefore, likely that the putative histidine mode that changes upon the S_1-to-S_2 and S_2-to-S_3 transitions reverses upon the S_0-to-S_1 transition. Apart from the histidine modes, there are several bands that changed their intensities depending on the S-state cycling; however, the dependency for some of these bands was not distinctively observed in the difference spectra shown in Figure 3A. Although the 1184(+)/1173(−) cm^{-1} bands in the difference spectra in Figure 3A (spectra a) exhibited some S-state dependency, their changes were inexplicit because of the presence of the S-state-independent negative band near 1173 cm^{-1} after the second, third, and fourth flashes. In contrast, these bands appeared prominently in the $^{14}N/^{15}N$ double-difference spectrum for S_2/S_1 as the 1186(+)/1178(−) cm^{-1} differential band that revealed distinct changes upon the S-state cycling. The bands were absent in the double-difference spectrum for S_3/S_2 but evident with opposite signs for S_0/S_3, and then they disappeared again for S_1/S_0.

The difference spectra for the S-state cycling of *Synechocystis* in the 1000−800 cm^{-1} range and the effects of universal ^{15}N- (panel A) and ^{13}C-labeling (panel B) on the spectra are shown in Figure 5. FTIR measurements were conducted under experimental conditions identical to those used in the 1700−1080 cm^{-1} region, with the exception of the use of a 9.5-μm long-pass filter to improve the signal-to-noise ratio of the 1000−800 cm^{-1} spectra. The S_2/S_1 spectrum of the unlabeled *Synechocystis* (red lines) showed major bands at 945(+), 922(−), 870(−), 854(+), 845(−), 822(+), and 812(+) cm^{-1} and less intense bands at 980(+), 960(−), 910(+), and 895(+) cm^{-1}. Among them, the 854(+), 845(−), 822(+), and 812(+) cm^{-1} bands showed flash-number-dependent changes and were similarly induced in the fifth-flash spectra despite having reduced intensities (data not shown). The resulting S_2/S_1 spectrum is roughly comparable to the previously reported spectrum of spinach PS II core particles, although bands other than those at 860(+), 850(−), and 820(+) cm^{-1} were not resolved in it (*25*). Upon ^{15}N-labeling, bands in the range of 1000−900 cm^{-1} were considerably affected, whereas the bands at 870(−), 854(+), 845(−), 822(+), and 812(+) cm^{-1} were only slightly affected. Upon ^{13}C-labeling, significant downward shifts were observed for most of the S_2/S_1 bands, including the ^{15}N-insensitive bands in the 900−800 cm^{-1} region. Accordingly, the 900−800 cm^{-1} bands are attributable to the carbon-containing but not the nitrogen-containing groups. Several bands in the 1000−900 cm^{-1} region were affected by both isotopes and therefore can be assigned to the vibrational modes of the amino acid side chains that contain both carbon and nitrogen atoms since none of the protein modes are expected to appear in this frequency region (*49*). The spectrum after the second, third, or fourth flash was considerably different from the S_2/S_1 spectrum. However, in contrast to the spectra in the 1700−1300 (Figure 2) and 1300−1080 cm^{-1} (Figure 3) regions, only a few bands showed distinct S-state dependency. One may presume that the higher S-state is scrambling due to nonoptimal excitation of the samples for the measurements of the 1000−800 cm^{-1} spectra. However, this is not the case because the 1700−1080 and 1000−800 cm^{-1} spectra were measured under

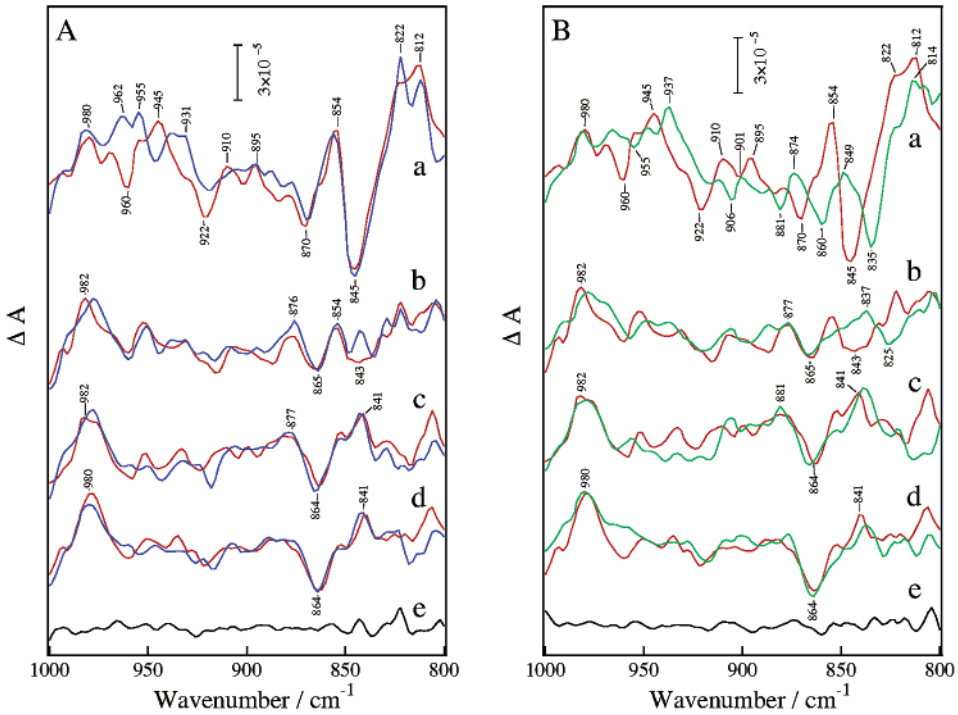

FIGURE 5: Effects of ^{15}N- (panel A) and ^{13}C-labeling (panel B) on the flash-induced FTIR difference spectra in the frequency region of 1000−800 cm^{-1} of PS II core particles from *Synechocystis* sp. PCC 6803. (a) S_2/S_1, (b) S_3/S_2, (c) S_0/S_3, and (d) S_1/S_0 difference spectra induced upon the first-, second-, third-, and fourth-flash illumination of unlabeled (red lines), ^{15}N-labeled (blue lines), and ^{13}C-labeled (green lines) PS II core particles, respectively. Spectra e are presented to show the noise levels.

identical conditions, with the exception of the difference in the cutoff wavenumber of the Ge filter, as described in the Materials and Methods section. In fact, 1000−800 cm^{-1} S-state spectra with identical spectral features were observed despite having lower quality when the 1700−800 cm^{-1} spectra were measured using 6-μm long-pass filter (data not shown).

The intensity of the prominent 854(+)/845(−) cm^{-1} bands in the unlabeled S_2/S_1 spectrum decreased with the same sign in the S_3/S_2 spectrum. These bands, however, seemed to appear with the opposite sign in the S_0/S_3 and S_1/S_0 spectra. Unfortunately, the S-state-dependent behavior of the 854(+) cm^{-1} band was rather ambiguous due to the presence of a prominent band at 865(−) cm^{-1}. This negative band was scarcely induced after the first flash but appeared constantly after the second and successive flashes and was insensitive to ^{15}N- and ^{13}C-labeling. The isotope-insensitive band at 980(+) cm^{-1} was similarly induced in all difference spectra. These bands may be attributable to some light-induced changes that are not directly related to the PS II components, such as proton uptake by the buffer molecules.

To minimize the contribution from components other than PS II, we calculated the $^{14}N/^{15}N$ and $^{12}C/^{13}C$ double-difference spectrum for each S-state transition in the range of 1000−800 cm^{-1} by subtracting the isotope-labeled S-state difference spectra from the unlabeled ones. The results are shown in Figure 6. The $^{14}N/^{15}N$ double-difference spectra (panel A) showed that several ^{15}N-sensitive bands at 962(−), 945(+), 931(−), 922(−), and 910(+) cm^{-1} were induced in the spectrum for the S_2/S_1 difference (spectrum a). However, bands corresponding to these were not apparent in the spectra for the S_3/S_2 (spectrum b), S_0/S_3 (spectrum c), and S_1/S_0 difference (spectrum d). The $^{12}C/^{13}C$ double-difference spectra (panel B) showed more bands as compared with those for the $^{14}N/^{15}N$ double-difference. Among them, the bands near 847(−), 833(+), and 822(+) cm^{-1} seemed to change sign and intensity in the double-difference spectra for the S_3/S_2 (spectrum b) and S_0/S_3 difference (spectrum c), but the presence of the isotopic bands was not obvious in the spectrum for the S_1/S_0 difference (spectrum d) due to rather high background noise resulting from the double subtraction (spectrum e). Although other bands seem to be showing the S-state dependency, the relatively lower spectral quality prevented us from inspecting those bands closely. These results indicate that the carbon-containing but not nitrogen-containing groups of the PS II components are predominantly responsible for the S-state-dependent bands at 850−820 cm^{-1}.

The light-minus-dark difference spectra of the PS II core particles from *Synechocystis* are shown in Figure 7, in which the sample cores were illuminated with a single flash under conditions that preferentially induce the oxidation of the Mn cluster from S_1 to S_2 (spectrum a) or Y_D tyrosine (spectrum d) and the reduction of Q_A (spectrum b) or the non-heme iron (spectrum c). Except for some minor differences in the peak positions and relative band intensities, the resulting spectra in the 1700−1080 cm^{-1} region (panel A) were comparable to the previously reported Q_A^-/Q_A (*24*, *25*), Fe^{2+}/Fe^{3+} (*17*, *18*), and $Y_D^{\bullet}/Y_D$ (*20*, *21*) spectra. The absence of the typical CO stretching mode of Q_A^- at 1477(+) cm^{-1} clearly demonstrated the absence of any contributions of the Q_A^-/Q_A bands to the S_2/S_1 spectrum. In addition, the S_2/S_1 spectrum scarcely showed the 1103(−) cm^{-1} band, which has been assigned to the side-chain modes from the histidine ligands of the non-heme iron. This, therefore, indicated only minor contributions of the Fe^{2+}/Fe^{3+} band to the S_2/S_1 spectrum. Although several bands that appeared in the $Y_D^{\bullet}/Y_D$ spectrum (spectrum d) seemed to be present in the S_2/S_1

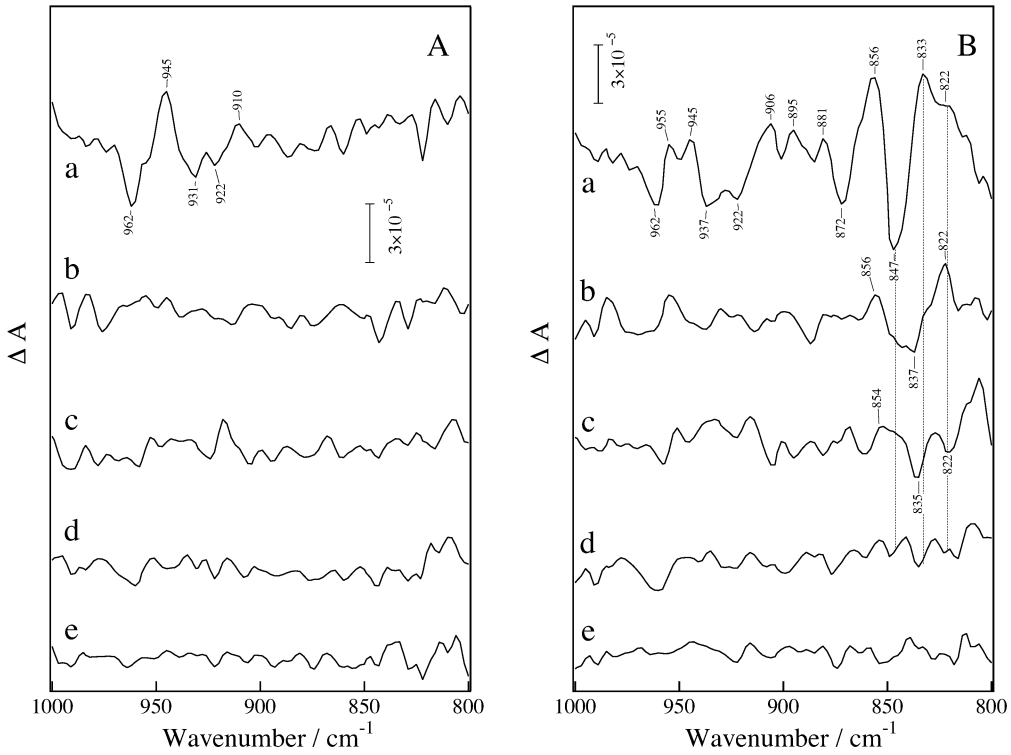

FIGURE 6: $^{14}N/^{15}N$ (panel A) and $^{12}C/^{13}C$ (panel B) double-difference spectra of PS II core particles from *Synechocystis* sp. PCC 6803 for the S-state cycling. Double-difference spectra for (a) S_2/S_1, (b) S_3/S_2, (c) S_0/S_3, and (d) S_1/S_0 difference. The $^{14}N/^{15}N$ or $^{12}C/^{13}C$ double-difference spectra were obtained by subtracting ^{15}N- or ^{13}C-labeled S-state difference spectra from unlabeled S-state difference spectra. Spectra e are presented to show the noise levels for the double subtraction.

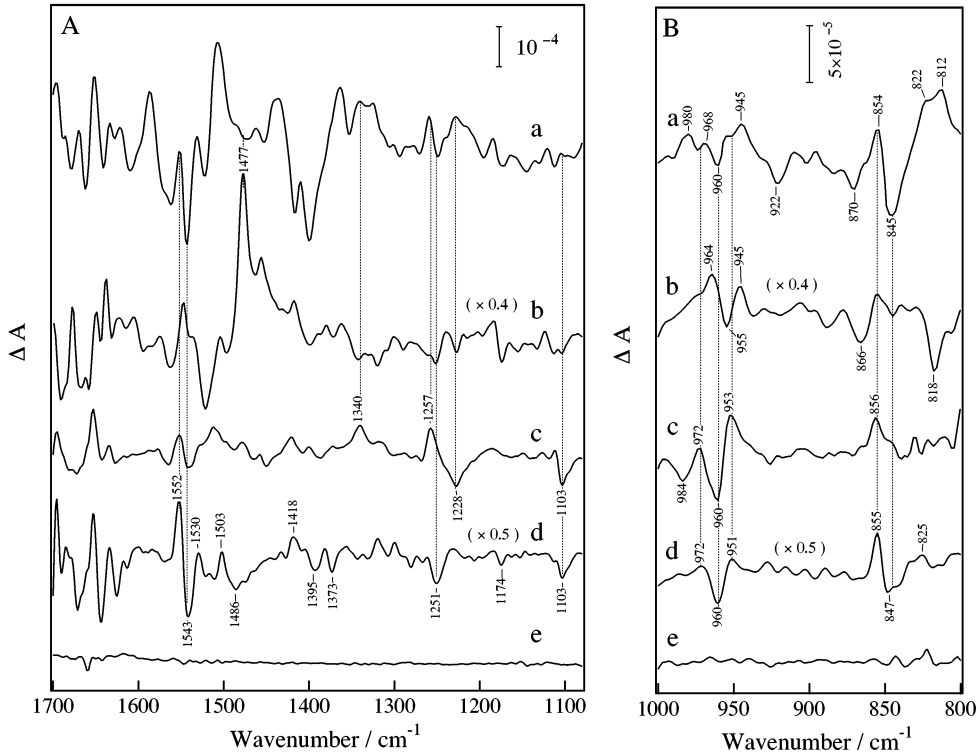

FIGURE 7: Flash-induced (a) S_2/S_1, (b) Q_A^-/Q_A, (c) Fe^{2+}/Fe^{3+}, and (d) $Y_D^\bullet/Y_D$ difference spectra of PS II core particles from *Synechocystis* in the frequency range of 1700−1080 cm^{-1} (panel A) and 1000−800 cm^{-1} (panel B). Samples cores were illuminated with a single-pulse from a frequency-doubled Nd^{3+}:YAG laser (532 nm, 6−7 ns, 10 mJ/cm^2/pulse) at 273 K. Spectra a in panels A and B are reproductions of spectrum a (black line) of Figure 1 and spectrum a (red line) of Figure 5, respectively. See text for details of conditions for respective measurements.

spectrum (spectrum a), the distinct 1103(−) cm^{-1} band in the $Y_D^\bullet/Y_D$ spectrum was not detected in the S_2/S_1 spectrum, which may suggest that the $Y_D^\bullet/Y_D$ modes are not involved in the spectrum. However, we cannot completely exclude the contribution of the $Y_D^\bullet/Y_D$ bands from the present results since the 1103(−) cm^{-1} band may not be necessarily ascribed

to the $Y_D^{\bullet}/Y_D$ mode (*21*). Nevertheless, the contribution of the $Y_D^{\bullet}/Y_D$ bands to the S_2/S_1 spectrum seems negligibly small since apparent differences were not observed in the S_2/S_1 spectra between the wild-type and Y_D-less *Synechocystis* (unpublished results). Accordingly, we can conclude that the obtained S_2/S_1 spectrum has eliminated the bands from the Q_A^-/Q_A, Fe^{2+}/Fe^{3+}, and $Y_D^{\bullet}/Y_D$ spectra, and therefore, redox reactions of Q_A, non-heme iron, and Y_D do not occur upon illumination under the present conditions.

As shown in panel B of Figure 7, the Q_A^-/Q_A spectrum (spectrum b) in the 1000−800 cm^{-1} region showed prominent bands at 964(+), 955(−), 945(+), 866(−), 854(+), and 818(−) cm^{-1} which were comparable to those previously reported for spinach (*25*). The Fe^{2+}/Fe^{3+} (spectrum c) and $Y_D^{\bullet}/Y_D$ spectra (spectrum d) showed the characteristic features; several bands in the 975−945 cm^{-1} region similarly appeared in the Q_A^-/Q_A, Fe^{2+}/Fe^{3+}, and $Y_D^{\bullet}/Y_D$ spectra, although the positions and the relative intensities of the bands were not necessarily coincident. The results may imply that the bands are ascribed to amino acid residues which exist commonly in the proximity of these redox components. The bands at 854(+) and/or 960(−) cm^{-1} are similarly induced in the S_2/S_1, Q_A^-/Q_A, Fe^{2+}/Fe^{3+}, and $Y_D^{\bullet}/Y_D$ spectra. However, none of the redox changes of Y_D, non-heme iron, and Q_A is responsible for these bands in the S_2/S_1 spectrum, since the illumination does not induce the redox reactions of these components as depicted in the mid-frequency spectra shown in panel A.

DISCUSSION

S-State Spectra in the 1700−1300 cm^{-1} Range. The mid-frequency FTIR difference spectra for the S-state cycling have been reported for the PS II cores from thermophilic cyanobacterium (*Thermosynechococcus*) (*30*, *36*, *39*, *40*) and BBY-type PS II membranes from higher plant (spinach) (*31*), and possible assignments of the detected bands have been discussed in detail. The present study showed that FTIR difference spectra for respective S-state transitions were basically compatible between the PS II cores from *Synechocystis* and spinach, although slight differences were found in the peak positions and band intensities. Furthermore, these spectra also showed striking similarity with those obtained for *Thermosynechococcus* (*30*, *36*, *39*, *40*). These results strongly indicate that the oxygen evolution occurs through largely identical processes, despite the subtle conformational differences in the protein moieties between cyanobacteria and higher plants. It was reported that bands at 1717(+), 1567(−), and 1401(−) cm^{-1} were induced by the protonation of carboxylate groups from the PS II protein when the pH was decreased during the repetitive S-state cyclings (*30*, *36*). These bands were not induced under the present experimental conditions (Figure 1 and unpublished data).

Among the S-state-dependent bands, the behaviors of the symmetric carboxylate stretching modes during the S-state cycling are particularly of interest since the structural changes of the putative carboxylate ligands for the Mn cluster can be monitored with minimal interferences from other vibrational modes. A typical S_2/S_1 carboxylate band at 1438(+), 1417(−), 1400(−), 1340(+), or 1325(+) cm^{-1} (see Figure 1) was observed at nearly the same position with the same sign and lower intensity in the S_3/S_2 spectrum, but with the opposite sign in the S_0/S_3 and S_1/S_0 spectra. This S-state dependency of the bands cannot be explained by assuming a single carboxylate group because the change in force constant of the carboxylate upon the Mn oxidation should be accompanied by the shift of the band. Therefore, the results suggested that each band's behavior during the S-state cycling is attributable to several individual carboxylate groups with similar force constants, which change equally upon every S-state step, although the number of the responsible carboxylate groups changes depending on the respective transition steps. On the other hand, the carboxylate bands at 1383(−) and 1363(+) cm^{-1} changed characteristically with S-state dependency that was different from that of the 1438(+), 1417(−), 1400(−), 1340(+), and 1325(+) cm^{-1} bands, indicating that the two bands at 1383(−) and 1363(+) cm^{-1} are attributable to distinct carboxylate groups that respond differently to the S-state transitions. It has been reported that, in the case of *Synechocystis*, upon L-[1-^{13}C]alanine-labeling, the 1320(+)/1356(−) cm^{-1} bands in the S_2/S_1 spectrum of the unlabeled PS II cores shifted downward by 16−18 cm^{-1} to 1304(+)/1338(−) cm^{-1} (*34*). These bands may correspond to the 1325(+)/1354(−) cm^{-1} bands in the unlabeled S_2/S_1 spectrum (Figure 2A, red line) and to the 1306(+)/1340(−) cm^{-1} band in the ^{13}C-labeled S_2/S_1 spectrum (Figure 2B, green line); however, the isotopic band at 1338(−) cm^{-1} was not distinctively resolved, presumably due to the concurrent isotope shifts of other carboxylate bands. Therefore, it is likely that the 1325(+)/1354(−) and/or 1340(+) cm^{-1} bands may be ascribed to the symmetric carboxylate stretching modes of the C-terminal Ala-344, which is assumed to be a ligand for the Mn cluster. Interestingly, the replacement of Ala-344 of the D1 protein with Gly affected the 1354(−) cm^{-1} band (unpublished result).

S-State Spectra in the 1300−1080 cm^{-1} Range. It is known that the weak amide III mode, including the CN stretching and NH bending modes of the polypeptide backbone, appears at 1300−1225 cm^{-1} (*49*). However, in the 1300−1200 cm^{-1} region, considerably smaller isotopic shifts due to ^{15}N-labeling rather than ^{13}C-labeling indicated that the contribution of the amide III mode to the spectra is very small. Therefore, a large part of the bands at 1300−1225 cm^{-1} can be assigned to the modes from amino acid side chains containing nitrogen and carbon. As shown in Figure 3, the band appeared positively in the S_3/S_2 and negatively in the S_0/S_3 and S_1/S_0 spectra at 1255 cm^{-1}, whereas none of the bands were distinct in the S_2/S_1 spectrum. Despite a slight difference in the peak position, similar S-state dependence for this mode was found in spinach PS II cores, as shown in Figure 1. Therefore, the 1255 cm^{-1} band may be the mode closely associated with the S-state. Our results show that this band was insensitive to ^{15}N-labeling but exhibited a significant downward shift upon ^{13}C-labeling, indicating that the band arises from a group containing carbon but not nitrogen. The 1254(−) cm^{-1} (1255(−) cm^{-1} in this study) band, which was obstructed by the 1260(+)/1246(−) cm^{-1} bands (1259(+)/1248(−) cm^{-1} in this study) in the S_2/S_1 spectrum, was assigned to the COH bending and/or CO stretching modes of the tyrosine residue coupled to the Mn cluster (*20*, *23*). Therefore, a candidate for the 1255 cm^{-1} band is the Y_Z mode that is closely related to the OEC during S-state cycling. It is of note in this context that the 1263(+),

1254(−), and 1235(+) cm^{-1} bands were induced upon the lowering of the buffer pH without PS II samples (data not shown), suggesting that a small part of the bands insensitive to either isotope labeling may correspond to the proton release/uptake by the buffer molecules, such as Mes.

The bands at 1196(−), 1184(+), 1163(+), 1146(−), and 1105(+) cm^{-1} showed changes in their sign and intensity depending on the flash number, thus indicating that these bands are involved in the S-state processes. The 1146(−) cm^{-1} band was influenced only upon ^{13}C-labeling, suggesting that this band is derived from carbon-containing but not nitrogen-containing group, such as C−O stretching modes of Asp, Glu, and/or Thr or CH_2-twisting modes from some alkyl groups (*50*). On the other hand, the 1196(−), 1184(+), and 1163(−) cm^{-1} bands shifted downward by 4 and 11−19 cm^{-1} upon ^{15}N- and ^{13}C-labeling, respectively. These bands, therefore, are attributable to the nitrogen- and carbon-containing amino acid side chain(s), such as His, Arg, Trp, or Lys. Among these amino acids, Lys is an unlikely candidate because of the relatively low IR intensities of the bands from Lys side chains (*50*−*52*). The CN stretching vibrations of monoalkylguanidinium give bands at 1180−1170 cm^{-1} which show a downward shift of 4 cm^{-1} upon ^{15}N-labeling of the two nitrogen atoms in the guanidinium group (*53*). Accordingly, some of the bands at 1196−1163 cm^{-1} may be ascribed to Arg. In addition, the symmetric and asymmetric stretching vibrations of the guanidinium group appear at 1685−1655 and 1635−1615 cm^{-1}, respectively, which show downward shifts of 6−9 cm^{-1} upon ^{15}N-labeling (*53*). The unlabeled S_2/S_1 spectrum showed bands at 1680(−), 1670(+), and 1610(−) cm^{-1} which shifted downward by 4 cm^{-1} upon ^{15}N-labeling and showed S-state dependency (Figure 2A). Accordingly, despite the relatively small ^{15}N-dependent downward shifts, these bands may be attributable to the modes of Arg. It has been reported that the 1668(+) cm^{-1} (1670(+) cm^{-1} in this study) band in the S_2/S_1 spectrum was specifically suppressed when the functional Cl^- site was occupied by monovalent anions (CH_3COO^-, I^-, Br^-, and Cl^- in order of band suppression) (*38*). Interestingly, this trend is compatible with that of anion effectiveness, which induced the characteristic shifts of the CN stretching modes of the guanidino group in ethylguanidinium salts (*53*). Based on the results, a possible interpretation is that the band is ascribed to Arg residue, which participates in the binding of Cl^-.

The S_2/S_1 band at 1113(−) cm^{-1} has been assigned to the CN stretching mode of the putative histidine ligand for the Mn cluster (*26*). The band showed downward shifts upon ^{15}N- and ^{13}C-labeling similar to those shown in Figure 3. Close inspection of the isotopic bands revealed that the ^{15}N- and ^{13}C-effected bands appear at 1107 ($\Delta = -6$ cm^{-1}) and 1105 cm^{-1} ($\Delta = -8$ cm^{-1}), respectively, with good reproducibility. The small difference between the isotopic shifts can be reasonably explained by the fact that the isotopic effect on the CN stretching mode is slightly smaller for $^{14}N/^{15}N$ than for $^{12}C/^{13}C$ due to the difference in their reduced masses. Furthermore, the isotopic bands seemed to change their sign and intensity in an S-state-dependent manner, as shown in the $^{14}N/^{15}N$ double-difference spectra (see Figure 4), supporting the view that the mode of the histidine ligand for the Mn cluster is responsible for the band. The mode appeared as a positive band in the S_1/S_0 spectrum and as a negative band in the S_2/S_1 and S_3/S_2 spectra, but was not discernible in the S_0/S_3 spectrum. This band behavior suggests that the appearance of the histidine band is not a simple reflection of the oxidation of the coordinating Mn ion but is ascribed to structural and/or chemical changes of the interactions between the histidine ligand and the Mn cluster during water oxidation. On the other hand, the origin of the isotope-insensitive 1113(−) cm^{-1} band, which appeared constantly after the second, third, and fourth flashes, may be ascribed to the buffer molecules in the FTIR samples. Although this band was relatively small in the spectrum after the fifth flash, the intensities of the bands induced after the sixth, seventh, and eighth flashes were comparable to those induced after the second, third, and fourth flashes (unpublished data). If this implies band induction upon S_2-to-S_3, S_3-to-S_0, and S_0-to-S_1 but not S_1-to-S_2 transitions, then a plausible interpretation is that the band reflects the structural changes of the buffer molecule due to the proton released from the OEC, although the band intensity for each transition may not correspond to the quantity of the proton owing to the scrambling of the higher S-state.

S-State Spectra in the 1000−*800 cm*$^{-1}$ *Range*. In the S_2/S_1 spectrum, the prominent bands in the 900−800 cm^{-1} region were affected only by ^{13}C-labeling, whereas the medium-intensity bands in the 1000−900 cm^{-1} region were sensitive to both isotopes, as clearly depicted in the $^{14}N/^{15}N$ and $^{12}C/^{13}C$ double-difference spectra shown in Figure 6, where possible contributions from buffer molecules were excluded. Since the contribution from Q_A^-/Q_A, Fe^{2+}/Fe^{3+}, and $Y_D^{\bullet}/Y_D$ bands to the flash-induced S_2/S_1 difference spectrum can be negligible, as shown from both the mid-frequency and mid- to low-frequency FTIR spectra (Figure 7), the bands observed in the S_2/S_1 spectrum can be attributed to the consequences of the oxidation of the Mn cluster upon the S_1-to-S_2 transition, which includes the structural changes of the amino acid side chains and/or the backbone polypeptides. Although a weak protein mode due to the symmetric CNC stretching vibration generally appears in the frequency region of 900−800 cm^{-1} (*49*), this is not the case since the ^{13}C-sensitive bands at 870(−), 854(+), 845(−), 822(+), and 812(+) cm^{-1} showed minimal ^{15}N-induced isotope shifts. Therefore, the ^{13}C-sensitive S-state-dependent bands at the 850−820 cm^{-1} range in Figure 6B may be attributable to the modes of amino acid side chains that are free of nitrogen atoms. A possible assignment for these modes includes out-of-plane CH vibrations of aromatic rings (*49*), such as those of Tyr and Phe. The 1254(−) cm^{-1} (1255(−) cm^{-1} in this study) band hidden in the S_2/S_1 spectrum has been assigned to the mode of tyrosine that is structurally coupled with the Mn cluster (*20*). Taking into account our unpublished result that Y_D deficiency did not affect the mid- to low-frequency S_2/S_1 spectrum, the tyrosine Y_Z mode may be included in the 900−800 cm^{-1} bands. It has been suggested that the ^{13}C-sensitive S-state-dependent bands at 3148 and 3130 cm^{-1} can be ascribed to the CH stretching modes of an imidazole group of His (*40*). Therefore, the CH wagging modes of the imidazole ring of the His side chains (*54*) may be another possible candidate for the^{13}C-sensitive bands that show the S-state dependency in the 900−800 cm^{-1} region.

Although the spectra for the 1000−800 cm^{-1} region changed depending on the flash number, their S-state dependence in terms of respective IR bands was not clear

as compared with the spectra in the 1700−1080 cm^{-1} region. The presence of the anomalous bands and extensive overlaps of many small bands in this frequency region may be the inherent reason for the absence of a clear S-state dependence for the observed bands. Generally, the interactions between Mn ions and water molecules are detectable in the frequency range of 900−300 cm^{-1} (*25*, *44*, *45*). However, the 1000−800 cm^{-1} spectra were scarcely affected by the $H_2{}^{18}O$ substitution (unpublished results), suggesting that the vibrational modes from the Mn−water interactions in the OEC are undetectable or entirely absent in this frequency region. Amino-acid-specific isotope labeling will help further characterize the observed bands. The 980(+) and 865(−) cm^{-1} bands appeared with the same sign during the S-state cycling and were not influenced by the isotope labeling, indicating that these bands originated from some components other than those of PS II due to the consequences of the S-state transitions indirectly. Some changes of buffer molecules, such as the protonation of Mes, are presumed to be responsible for these bands.

REFERENCES

1. Debus, R. J. (1992) The manganese and calcium ions of photosynthetic oxygen evolution, *Biochim. Biophys. Acta 1102*, 269−352.
2. Witt, H. T. (1996) Primary reactions of oxygen photosynthesis, *Ber. Bunsen-Ges. Phys. Chem. 100*, 1923−1942.
3. Hoganson, C. W., and Babcock, G. T. (2000) Mechanistic aspects of the tyrosyl radical-manganese complex in photosynthetic water oxidation, *Met. Ions Biol. Syst. 37*, 613−656.
4. Renger, G. (2001) Photosynthetic water oxidation to molecular oxygen: apparatus and mechanism, *Biochim. Biophys. Acta 1503*, 210−228.
5. Yocum, C. F. (1991) Calcium activation of photosynthetic water oxidation, *Biochim. Biophys. Acta 1059*, 1−15.
6. Zouni, A., Witt, H.-T., Kern, J., Fromme, P., Krauss, N., Saenger, W., and Orth, P. (2001) Crystal structure of photosystem II from *Synechococcus elongatus* at 3.8 Å resolution, *Nature 409*, 739−743.
7. Fromme, P., Kern, J., Loll, B., Biesiadka, J., Saenger, W., Witt, H. T., Krauss, N., and Zouni, A. (2002) Functional implications on the mechanism of the function of photosystem II including water oxidation based on the structure of photosystem II, *Philos. Trans. R. Soc. London Ser. B 357*, 1337−1345.
8. Kamiya, N., and Shen, J.-R. (2003) Crystal structure of oxygen-evolving photosystem II from *Thermosynechococcus vulcanus* at 3.7-Å resolution, *Proc. Natl. Acad. Sci. U.S.A. 100*, 98−103.
9. Hillier, W., and Wydrzynski, T. (2001) Oxygen ligand exchange at metal sites−implications for the O_2 evolving mechanism of photosystem II, *Biochim. Biophys. Acta 1503*, 197−209.
10. Geijer, P., Peterson, S., Åhrling, K. A., Deák, Z., and Styring, S. (2001) Comparative studies of the S_0 and S_2 multiline electron paramagnetic resonance signals from the manganese cluster in Photosystem II, *Biochim. Biophys. Acta 1503*, 83−95.
11. Peloquin, J. M., and Britt, R. D. (2001) EPR/ENDOR characterization of the physical and electronic structure of the OEC Mn cluster, *Biochim. Biophys. Acta 1503*, 96−111.
12. Robblee, J. H., Cinco, R. M., and Yachandra, V. K. (2001) X-ray spectroscopy-based structure of the Mn cluster and mechanism of photosynthetic oxygen evolution, *Biochim. Biophys. Acta 1503*, 7−23.
13. Yachandra, V. K. (2002) Structure of the manganese complex in photosystem II: insights from X-ray spectroscopy, *Philos. Trans. R. Soc. London Ser. B 357*, 1347−1358.
14. Saygin, Ö., and Witt, H. T. (1987) Optical characterization of intermediates in the water-splitting enzyme system of photosynthesis−possible states and configurations of manganese and water, *Biochim. Biophys. Acta 893*, 452−469.
15. Noguchi, T., Ono, T.-A., and Inoue, Y. (1992) Detection of structural changes upon S_1-to-S_2 transition in the oxygen-evolving manganese cluster in photosystem II by light-induced Fourier transform infrared difference spectroscopy, *Biochemistry 31*, 5953−5956.
16. Noguchi, T., Ono, T.-A., and Inoue, Y. (1995) Direct detection of a carboxylate bridge between Mn and Ca^{2+} in the photosynthetic oxygen-evolving center by means of Fourier transform infrared spectroscopy, *Biochim. Biophys. Acta 1228*, 189−200.
17. Noguchi, T., and Inoue, Y. (1995) Identification of Fourier transform infrared signals from the non-heme iron in photosymtem II, *J. Biochem. 118*, 9−12.
18. Hienerwadel, R., and Berthomieu, C. (1995) Bicarbonate binding to the non-heme iron of photosystem II investigated by Fourier transform infrared difference spectroscopy and ^{13}C-labeled bicarbonate, *Biochemistry 34*, 16288−16297.
19. Zhang, H., Razeghifard, M. R., Fischer, G., and Wydrzynski, T. (1997) A time-resolved FTIR difference study of the plastoquinone Q_A and redox-active tyrosine Y_Z interactions in photosystem II, *Biochemistry 36*, 11762−11768.
20. Noguchi, T., Inoue, Y., and Tang, X.-S. (1997) Structural coupling between the oxygen-evolving Mn cluster and a tyrosine residue in photosystem II as revealed by Fourier transform infrared spectroscopy, *Biochemistry 36*, 14705−14711.
21. Hienerwadel, R., Boussac, A., Breton, J., Diner, B. A., and Berthomieu, C. (1997) Fourier transform infrared difference spectroscopy of photosystem II tyrosine D using site-directed mutagenesis and specific isotope labeling, *Biochemistry 36*, 14712−14723.
22. Zhang, H., Fischer, G., and Wydrzynski, T. (1998) Room-temperature vibrational difference spectrum for $S_2Q_B^-/S_1Q_B$ of photosystem II determined by time-resolved Fourier transform infrared spectroscopy, *Biochemistry 37*, 5511−5517.
23. Berthomieu, C., Hienerwadel, R., Boussac, A., Breton, J., and Diner, B. A., (1998) Hydrogen bonding of redox-active tyrosine Z of photosystem II probed by FTIR difference spectroscopy, *Biochemistry 37*, 10547−10554.
24. Noguchi, T., Inoue, Y., and Tang, X.-S. (1999) Hydrogen bonding interaction between the primary quinone acceptor Q_A and a histidine side chain in photosystem II as revealed by Fourier transform infrared spectroscopy, *Biochemistry 38*, 399−403.
25. Chu, H.-A., Gardner, M. T., O'Brien, J. P., and Babcock, G. T. (1999) Low-frequency Fourier transform infrared spectroscopy of the oxygen-evolving and quinone acceptor complexes in photosystem II, *Biochemistry 38*, 4533−4541.
26. Noguchi, T., Inoue, Y., and Tang, X.-S. (1999) Structure of a histidine ligand in the photosynthetic oxygen-evolving complex as studied by light-induced Fourier transform infrared difference spectroscopy, *Biochemistry 38*, 10187−10195.
27. Noguchi, T., and Sugiura, M. (2000) Structure of an active water molecule in the water-oxidizing complex of photosystem II as studied by FTIR spectroscopy, *Biochemistry 39*, 10943−10949.
28. Chu, H.-A., Sackett, H., and Babcock, G. T. (2000) Identification of a Mn−O−Mn cluster vibrational mode of the oxygen-evolving complex in photosystem II by low-frequency FTIR spectroscopy, *Biochemistry 39*, 14371−14376.
29. Chu, H.-A., Hillier, W., Law, N. A., Sackett, H., Haymond, S., and Babcock, G. T. (2000) Light-induced FTIR difference spectroscopy of the S_2-to-S_3 state transition of the oxygen-evolving complex in photosystem II, *Biochim. Biophys. Acta 1459*, 528−532.
30. Noguchi, T., and Sugiura, M. (2001) Flash-induced Fourier transform infrared detection of the structural changes during the S-state cycle of the oxygen-evolving complex in photosystem II, *Biochemistry 40*, 1497−1502.
31. Hillier, W., and Babcock, G. T. (2001) S-state dependent Fourier transform infrared difference spectra for the photosystem II oxygen evolving complex, *Biochemistry 40*, 1503−1509.
32. Chu, H.-A., Debus, R. J., and Babcock, G. T. (2001) D1-Asp170 is structurally coupled to the oxygen evolving complex in photosystem II as revealed by light-induced Fourier transform infrared difference spectroscopy, *Biochemistry 40*, 2312−2316.
33. Kimura, Y., and Ono T.-A. (2001) Chelator-induced disappearance of carboxylate stretching vibrational modes in S_2/S_1 FTIR spectrum in oxygen-evolving complex of photosystem II, *Biochemistry 40*, 14061−14068.
34. Chu, H.-A., Babcock, G. T., and Debus, R. J. (2001) Possible ligation of the Mn cluster in photosystem II by the carboxyl-terminus of the D1 polypeptide: an FTIR study, *Proceedings of the 12th International Congress on Photosynthesis*, S13-026, CSIRO Publishing, Collingwood, Australia.

35. Chu, H.-A., Hillier, W., Law, N. A., and Babcock, G. T. (2001) Vibrational spectroscopy of the oxygen-evolving complex and of manganese model compounds, *Biochim. Biophys. Acta 1503*, 69−82.
36. Noguchi, T., and Sugiura, M. (2002) Flash-induced FTIR difference spectra of the water oxidizing complex in moderately hydrated photosystem II core films: effect of hydration extent on S-state transitions, *Biochemistry 41*, 2322−2330.
37. Kimura, Y., Hasegawa, K., and Ono, T.-A. (2002) Characteristic changes of the S_2/S_1 difference FTIR spectrum induced by Ca^{2+} depletion and metal cation substitution in the photosynthetic oxygen-evolving complex, *Biochemistry 41*, 5844−5853.
38. Hasegawa, K., Kimura, Y., and Ono, T.-A. (2002) Chloride cofactor in the photosynthetic oxygen-evolving complex studied by Fourier transform infrared spectroscopy, *Biochemistry 41*, 13839−13850.
39. Noguchi, T., and Sugiura, M. (2002) FTIR detection of water reactions during the flash-induced S-state cycle of the photosynthetic water-oxidizing complex, *Biochemistry 41*, 15706−15712.
40. Noguchi, T., and Sugiura, M. (2003) Analysis of flash-induced FTIR defference spectra of the S-state cycle in the photosynthetic water-oxidizing complex by uniform ^{15}N and ^{13}C isotope labeling, *Biochemistry 42*, 6035−6042.
41. Kimura, Y., and Ono, T.-A. (2003) Functional and structural study on chelator-induced suppression of S_2/S_1 FTIR spectrum in photosynthetic oxygen-evolving complex, *J. Inorg. Biochem. 97*, 231−239.
42. Kimura, Y., Mizusawa, N., Ishii, A., Yamanari, T., and Ono, T.-A. (2003) Changes of low-frequency vibrational modes induced by universal ^{15}N- and ^{13}C-isotope labeling in S_2/S_1 FTIR difference spectrum of oxygen-evolving complex, *Biochemistry 42*, 13170−13177.
43. Hasegawa, K., Kimura, Y., and Ono, T.-A. (2004) Oxidation of the Mn cluster induces structural changes of NO_3^- functionally bound to the Cl^- site in the oxygen-evolving complex of photosystem II, *Biophys. J. 86*, 1042−1050.
44. Nakamoto, K. (1986) *Infrared and Raman Spectra of Inorganic and Coordination Compounds*, pp 53−57, Wiley, New York.
45. Zhou, M., Zhang, L., Shao, L., Wang, W., Fan, K., and Qin, Q. (2001) Reactions of Mn with H_2O and MnO with H_2. Matrix-isolation FTIR and quantum chemical studies, *J. Phys. Chem. A 105*, 5801−5807.
46. Berthold, D. A., Babcock, G. T., and Yocum, C. F. (1981) A highly resolved, oxygen-evolving photosystem II preparation from spinach thylakoid membranes, *FEBS Lett. 134*, 231−234.
47. Ono, T.-A., and Inoue, Y. (1986) Effects of removal and reconstitution of the extrinsic 33, 24 and 16 kDa proteins on flash oxygen yield in photosystem II particles, *Biochim. Biophys. Acta 850*, 380−389.
48. Shinkarev, V. P. (2003) Oxygen evolution in photosynthesis: simple analytical solution for the Kok model, *Biophys. J. 85*, 435−441.
49. Socrates, G. (1994) *Infrared and Raman Characteristic Group Frequencies*, *3rd ed*., pp 157−335, Wiley, Chichester.
50. Barth, A. (2000) The infrared absorption of amino acid side chains, *Prog. Biophys. Mol. Biol. 74*, 141−173.
51. Venyaminov, S. Y., and Kalnin, N. N. (1990) Quantitative IR spectrophotometry of peptide compounds in water (H_2O) solutions. I. Spectral parameters of amino acid residue absorption bands, *Biopolymers 30*, 1243−1257.
52. Rahmelow, K., Hübner, W., and Ackermann, Th. (1998) Infrared absorbances of ptotein side chains, *Anal. Biochem. 257*, 1−11.
53. Braiman, M. S., Briercheck, D. M., and Kriger, K. M. (1999) Modeling vibrational spectra of amino acid side chains in proteins: Effects of protonation state, counterion, and solvent on arginine C−N stretch frequencies, *J. Phys. Chem. B 103*, 4744−4750.
54. Hasegawa, K., Ono, T.-A., and Noguchi, T. (2000) Vibrational spectra and Ab initio DFT calculations of 4-methylimidazole and its different protonation forms: Infrared and Raman markers of the protonation state of a histidine side chain, *J. Phys. Chem. B 104*, 4253−4265.

BI0362323